POPULATION-SPECIFIC MODELLING OF BETWEEN/WITHIN-SUBJECT FLOW VARIABILITY IN THE CAROTID ARTERIES OF THE ELDERLY

TONI LASSILA, ALI SARRAMI-FOROUSHANI, SEYEDMOSTAFA HEJAZI, ALEJANDRO F. FRANGI

ABSTRACT. Computational fluid dynamics models are increasingly proposed for assisting the diagnosis and management of vascular diseases. Ideally, patient-specific flow measurements are used to impose flow boundary conditions. When patient-specific flow measurements are unavailable, mean values of flow measurements across small cohorts are used as normative values. In reality, both the between-subjects and within-subject flow variabilities are large. Consequently, neither one-shot flow measurements nor mean values across a cohort are truly indicative of the flow regime in a given person. We develop models for both the between-subjects and within-subject variability of internal carotid flow. A log-linear mixed effects model is combined with a Gaussian process to model the between-subjects flow variability, while a lumped parameter model of cerebral autoregulation is used to model the within-subject flow variability in response to heart rate and blood pressure changes. The model parameters are identified from carotid ultrasound measurements in a cohort of 103 elderly volunteers. Model utility is demonstrated in a computational study of intracranial aneurysm flow under rest and exercise.

Keywords – Computational fluid dynamics, cerebrovascular disease, patient-specific models, Gaussian process models, uncertainty quantification

1. INTRODUCTION

Numerous computational fluid dynamics (CFD) models of human cardio- and cerebrovascular physiology are published every year, but few of them make any impact in clinical practice. This inconvenient truth has been blamed on the improper use of CFD solvers [21], insufficient validation of biomechanics models [1], and lack of understanding of the clinical decision-making process by the biomedical engineers building the models [9]. One additional explanation is that many "patient-specific" CFD models fail to consider the physiological variability of vascular flow, confounding interpretation of model results and producing overly confident predictions of flow quantities. In our view, concentrated efforts should be made to identify both the magnitude of this variability and its effect on the predictions of vascular flow models [18].

Patient-specific modelling of vascular flow requires an accurate description of the lumen plus the definition of boundary conditions. The latter is done by measuring patient-specific flow waveforms using either phase contrast magnetic resonance imaging (pcMRI) or ultrasound-based flow measurement techniques. In case patient-specific flow measurements are not available, cohort-averaged values of flow from the literature

CENTRE FOR COMPUTATIONAL IMAGING & SIMULATION TECHNOLOGIES IN BIOMEDICINE (CISTIB), THE UNIVERSITY OF SHEFFIELD, PAM LIVERSIDGE BUILDING, NEWCASTLE STREET, SHEFFIELD S1 3JD, UNITED KINGDOM

E-mail address: a.frangi@sheffield.ac.uk.

are often used. For example, the small-scale studies [6, 8, 14] all used pcMRI to measure carotid flow in young healthy volunteers. The uncertainty caused by not knowing the exact patient-specific flow can also be quantified by running an ensemble of CFD simulations over a physiological range of flow variability. This allows the modeller to establish not only mean values but also variability bounds for the output quantities of interest. However, few large-scale studies have reported estimates of vascular flow variability in normal populations. There is a risk that mean values of flow in small cohorts are biased and almost certainly underestimate the physiological flow variability. This, in turn, will lead to overconfidence in vascular CFD uncertainty quantification.

The objectives of this study are: (i) identify key patient-specific vascular flow parameters, (ii) provide distributions of the flow parameters in a realistic elderly cohort, and (iii) develop data-driven and mechanistic models for both *between-subjects* and *within-subject* blood flow variability that explicitly incorporate demographic variables (age, sex, body size). Treatment of demographic variables is standard in biomedical studies, but relatively few attempts have been made so far to account for them in vascular flow models (see e.g. [2]). Our models will then provide: (i) cohort-specific boundary conditions to vascular CFD simulations in the case that patient-specific flow measurements are not available, and (ii) estimates of within-subject flow variability in cases where patient-specific flow measurements are available only as spot measurements.

Although the methods are general, to demonstrate the utility of the models we focus on internal carotid arterial (ICA) flow in the context of intracranial aneurysms. The flow in the left and right ICAs accounts for the majority of cerebral blood flow and is reported to have around 10-20% between-subjects variability in different studies [6, 12, 20]. Mean flow varies less within-subject due to the modulating effect of the cerebral autoregulation system, yet changes to the flow waveform can still be observed. In previous studies, it has been shown that changes in wall shear stress (WSS) induced by flow variability can significantly change the CFD-based predictions of intracranial aneurysm rupture risk [19, 25]. We consider within-subject flow variability induced by changes in systolic blood pressure (BP) and heart rate (HR) during physical exercise, and study the corresponding changes in WSS indicators, such as time-averaged WSS (TAWSS) or oscillatory shear index (OSI).

2. Materials and Methods

2.1. **Patient-specific vascular flow measurements.** Patient-specific carotid flow data (*Lido cohort*) used in this study were part of an Alzheimer's disease study conducted at the Istituto di Ricovero e Cura a Carattere Scientifico San Camillo, Lido di Venezia, Italy, and previously reported in [11]. The cohort included 103 elderly people (age 73 ± 7 years), of whom 53 were diagnosed with mild cognitive impairment and the rest were healthy controls. Exclusion criteria included cerebrovascular disease as main aetiology, as well as the presence of any cardiovascular disease. The cohort could, therefore, be identified as elderly but healthy from the standpoint of vascular disease. The study was approved by the joint ethics committee of the Health Authority Venice 12 and the IRCCS San Camillo (Protocol number 2014.08) and all participants gave informed consent prior to participation.

To measure carotid flow, ultrasound imaging (Siemens Acuson X300PE, Siemens Healthineers, Erlangen, Germany) was performed. Both left and right internal carotid

waveforms were digitised from the DICOM images using `im2graph` (Shai Vaingast, `www.im2graph.co.il`). Flow velocity signals were converted to flow rates by assuming a circular cross-section and fully developed flow. The resulting flow rate signals were normalised to unit time and synchronised so that the maximum systolic upstroke point was matched between all the signals.

2.2. **Statistical modelling of between-subjects variability in ICA flow.** We previously modelled between-subjects ICA flow variability in [19], where data from 17 healthy young adults [6] was used to train a Gaussian process model. In that work, the time-averaged mean flow rate was normalised for a given arterial diameter to achieve a time-averaged WSS of 1.5 Pa at the level of the carotid sinus. We extended this model to include also the between-subjects variability of the time-averaged flow.

The model was trained on log-transformed flow values to ensure that the predicted flow rates remained positive. The log-transformed ICA flow rates $q_{\text{ICA-L}}$ and $q_{\text{ICA-R}}$ were assumed to consist of two parts; the time-averaged mean flow, $\overline{y}_{bs}$, and the time-varying part (*waveform*), y^*_{bs}:

$$\begin{aligned} \log(q_{\text{ICA-L}}) &= \overline{y}_{bs,L} + y^*_{bs,L}, \\ \log(q_{\text{ICA-R}}) &= \overline{y}_{bs,R} + y^*_{bs,R}. \end{aligned} \tag{1}$$

For notational simplicity, we drop the indices L/R in what follows, keeping in mind that separate models were trained for both left and right carotid flow. The time-averaged part of the flow was modelled by a mixed-effects linear model:

$$\overline{y}_{bs} = \beta_0 + \beta_h x_{\text{height}} + \varepsilon = \beta_0 + \beta_h x_{\text{height}} + \sigma_{bs}\omega, \tag{2}$$

using height x_{height} as a fixed effect to account for the allometric dependence of cardiac output on body size [4]. The variance σ^2_{bs} was estimated from the residuals of the linear model fit, and $\omega \in \mathcal{N}(0,1)$ was the normal distribution. Separate effects were estimated for the male and female sub-cohorts.

The time-varying part of ICA flow, y^*_{bs}, was modelled as a Gaussian process:

$$y^*_{bs} = \mathcal{GP}(\sigma, t_i; \omega). \tag{3}$$

where $\{t_i\}_{i=1}^{\ell}$ were temporal landmarks that characterised the waveform shape. The flow rates at these landmark points were used to estimate the covariance matrix:

$$\Sigma = \begin{bmatrix} \Sigma^{LL} & \Sigma^{LR} \\ \Sigma^{RL} & \Sigma^{RR} \end{bmatrix}, \tag{4}$$

where $\Sigma^{LR}_{i,j} := \text{cov}\left[y^*_{bs,L}(t_j), y^*_{bs,R}(t_i)\right]$ is the covariance between the log-transformed left and right carotid waveforms $y^*_{bs,L}$, $y^*_{bs,R}$ (and similarly for the other sub-matrices). Again, the covariances were estimated separately for each sex. The between-subjects variability model fitting process is graphically represented in Fig. 1.

2.3. **Statistical modelling of within-subject variability in ICA flow.** Within-subject variability in ICA flow arises mainly due the changes in cardiac output, quantified here by heart rate (HR) and systolic blood pressure (SBP). These changes are modulated by the cerebral autoregulation system (CARS) that includes myogenic (pressure-driven), shear-induced (flow-driven), and metabolic (energy-driven) regulation mechanisms. To model within-subject variability of carotid flow, we considered a range of arterial BP

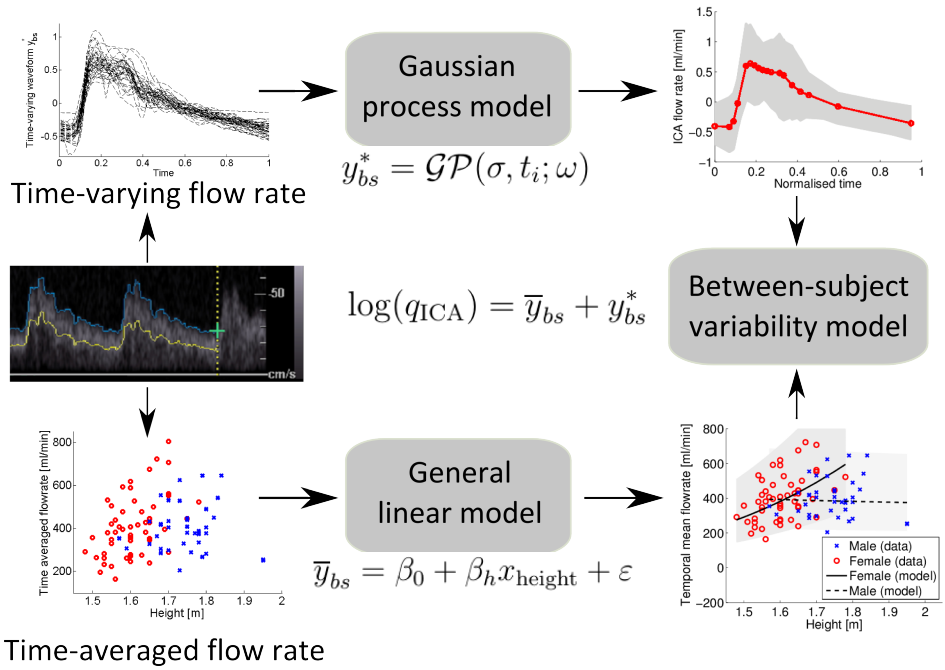

FIGURE 1. Training of the between-subjects flow variability -model (1).

waveforms with different values of HR and SBP and used a mathematical model of the CARS to generate the corresponding flow rate waveforms.

The CARS model of Mader *et al.* [13] is a two-element feedback controller, for which orthostatic stress tests were previously used to identify model parameters in both middle-aged and elderly volunteers:

$$\text{(5)} \qquad \begin{cases} \dfrac{dv_1}{dt} = -(a+b+c)v_1(t) + (c - d(t))v_2(t) + (a+b)p(t) \\ \dfrac{dv_2}{dt} = -bv_1(t) - dv_2(t) + bp(t) \\ d(t) = \dfrac{bcf_{aut}(t)}{Mc\,p(t) - (a+c)f_{aut}(t)} \\ f_{aut}(t) = 2.03 \cdot 10^{-6} p(t)^3 - 6.02 \cdot 10^{-4} p(t)^2 + 5.94 \cdot 10^{-2} p(t) - 1.95 \end{cases},$$

where the model parameters

$$\text{(6)} \qquad \begin{aligned} a &= a_m\lambda + (1-\lambda)a_e, & b &= b_m\lambda + (1-\lambda)b_e, \\ c &= c_m\lambda + (1-\lambda)c_e, & M &= M_m\lambda + (1-\lambda)M_e \end{aligned}$$

depended piecewise linearly on age x_{age}:

$$\text{(7)} \qquad \lambda = \begin{cases} 1, & \text{if } x_{\mathrm{age}} < 35 \\ \dfrac{75 - x_{\mathrm{age}}}{40}, & \text{if } 35 \le x_{\mathrm{age}} \le 75 \\ 0, & \text{if } x_{\mathrm{age}} > 75 \end{cases}$$

Finally, the flow velocity in the middle cerebral artery (MCA) was obtained as:

$$\text{(8)} \qquad v_{\mathrm{MCA}}(t) = M(p(t) - v_1(t)) + \overline{v},$$

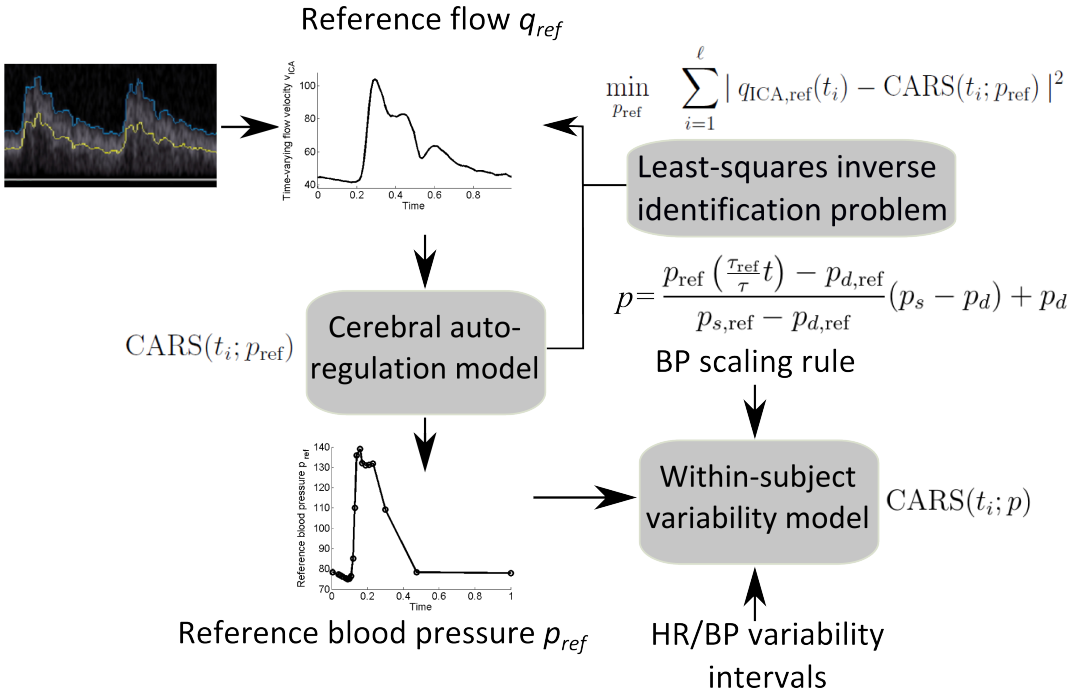

FIGURE 2. Training of the within-subject flow variability -model (5)–(8).

where $\overline{v}$ corresponds to the time-averaged flow velocity. To translate MCA flow velocities to ICA flow rates, we assumed a linear relationship between ICA and MCA flows:

$$q_{\rm ICA} = \gamma A_{\rm ICA} v_{\rm MCA}, \tag{9}$$

where $A_{\rm ICA}$ was the cross-sectional area of the ICA, and the VMCA/VICA index was $\gamma = 1.67 + 0.005 \times x_{\rm age}$ for women and $\gamma = 2.00$ for men, as proposed in [10].

To drive the CARS model, the BP waveform $p(t)$ needed to be specified. For a given reference HR, we assumed there exists a reference BP signal $p_{\rm ref}(t)$ with SBP $p_{s,\rm ref}$ and DBP $p_{d,\rm ref}$. The effect of HR and SBP variability on BP was then obtained by rescaling the reference BP waveform:

$$p(t; \tau, p_s, p_d) = \frac{p_{\rm ref}\left(\frac{\tau_{\rm ref}}{\tau} t\right) - p_{d,\rm ref}}{p_{s,\rm ref} - p_{d,\rm ref}}(p_s - p_d) + p_d. \tag{10}$$

where $\tau = 60/$ HR is the cardiac interval. Since BP waveforms were not available in this cohort, we used an inverse procedure to recover the reference BP from the ultrasound flow measurement by solving the least squares problem:

$$\min_{p_{\rm ref}} \quad \sum_{i=1}^{\ell} | \, q_{\rm ICA,ref}(t_i) - \mathrm{CARS}(t_i; p) \, |^2, \tag{11}$$

where $\mathrm{CARS}(t_i; p_{\rm ref})$ is the output of the CARS model at time t_i when driving the model with the reference pressure $p_{\rm ref}(t)$, and $q_{\rm ICA,ref}$ is the reference ICA flow waveform. The within-subject variability model fitting process is graphically represented in Fig. 2.

2.4. **Study on the effect of exercise on aneurysm flow.** To demonstrate the utility of intra-subject flow variability models, we studied the specific case of flow prediction in intracranial aneurysms (IAs). Aneurysms are vascular pathologies characterised by

the incremental growth of a saccular extrusion of the blood vessel that, over time, may rupture, leading to permanent morbidity or death. The mechanobiological growth and rupture process of IAs has been linked to changes in wall shear stress (WSS) patterns. A number of CFD studies [3, 19, 25] have looked at the effect of CBF fluctuations in WSS patterns, but none to our knowledge have considered the effect of the CARS. Quantities of interest include time-averaged WSS (TAWSS), oscillatory shear index (OSI), and transverse WSS (TransWSS):

$$\begin{aligned}
\mathrm{TAWSS}(x) &= \frac{1}{T_{\mathrm{period}}} \int_{T_0}^{T_0+T_{\mathrm{period}}} |\boldsymbol{\tau}_w(x,t)|\, dt; \\
\mathrm{OSI}(x) &= \frac{1}{2}\left(1 - \frac{\left|\int_{T_0}^{T_0+T_{\mathrm{period}}} \boldsymbol{\tau}_w(x,t)\, dt\right|}{\int_{T_0}^{T_0+T_{\mathrm{period}}} |\boldsymbol{\tau}_w(x,t)|\ dt}\right); \\
\mathrm{TransWSS}(x) &= \frac{1}{T_{\mathrm{period}}} \int_{T_0}^{T_0+T_{\mathrm{period}}} |\boldsymbol{\tau}_w(x,t) \cdot (\hat{p} \times \hat{n})|\ dt,
\end{aligned} \tag{12}$$

where $\hat{n}$ is the surface normal, and the unit vector $\hat{p}$ in the direction of the time-averaged WSS vector can be calculated as:

$$\hat{p}(x) = \frac{\int_{T_0}^{T_0+T_{\mathrm{period}}} \boldsymbol{\tau}_w(x,t)\, dt}{\left|\int_{T_0}^{T_0+T_{\mathrm{period}}} \boldsymbol{\tau}_w(x,t)\, dt\right|}. \tag{13}$$

To enable comparison of TransWSS across cases, we calculated the relative TransWSS (rTransWSS) as the TransWSS normalised by the TAWSS at each surface point [19]. All point-wise quantities were averaged over the aneurysmal sac and used for population-specific analyses. Previous studies indicate that endothelial regions at-risk of rupture can be characterised as having low TAWSS but highly fluctuating WSS (both high OSI and high TransWSS) [15]. As a sudden rise in blood pressure may trigger the rupture of an aneurysm [23, 24], we investigated whether changes in CBF experienced in hypertensive conditions play a role in altering the WSS patterns.

To generate a virtual cohort of IAs to test the differences in WSS between rest vs. exercise, patient-specific vascular surface models ($N = 54$) were segmented from previously acquired 3-D rotational angiography images in the @neurIST project [22]. Vascular models were discretised using unstructured volumetric meshes in ANSYS ICEM v16.2 (Ansys Inc., Canonsburg, PA, USA). Tetrahedral elements with maximum edge size of 0.2 mm were used and three layers of prismatic elements with an edge size of 0.1 mm were used to create boundary layers. Blood flow in the IA was modelled using the unsteady Navier–Stokes equations. Blood was assumed to be an incompressible Newtonian fluid with a density of 1066 kg/m^3 and viscosity of 0.0035 Pa·s. To ensure fully developed flow, the computational domain was extended at the inlet boundary by an entrance length proportional to the inlet boundary maximum Reynolds number. The Navier–Stokes equations were solved in ANSYS CFX v16.2 (Ansys Inc., Canonsburg, PA, USA). The cardiac cycle was discretised in time into 200 equal steps. Element and time-step sizes were set according to the neurIST processing toolchain where mesh and time-step size dependecy tests were performed on WSS, pressure, and flow velocity at several points in the computational domain as described by [22].

No patient-specific flow measurements were available in the @neurIST cohort. Instead, the mean waveform (different for men/women) from the Lido cohort was used as the baseline flow waveform. The baseline waveform was used as inlet boundary condition to the CFD models of aneurysm flow at rest. For each patient, obtain patient-specific physiologically-relevant flow waveforms and to enable population-wide comparisons, Poiseuille's law was used to scale the mean waveform such that the time-averaged WSS was 1.5 Pa at the inlet. We modeled differences between rest and exercise by increasing the HR from 66 bpm (at rest) to an elevated level of 145 bpm (during exercise), i.e., an increase by a factor of 2.2 [17]. These values were used as parameters in the within-subject flow variability model of Sect. 2.3. The baseline pressure waveform was determined for each case by solving problem (11). After solving the inverse problem, the systolic BP was correspondingly increased by a factor of 1.3 [17] in formula (10) to simulate effects of exercise and used to drive the CARS model and obtain the ICA waveform. The ICA waveforms where then used as inlet boundary condition to the CFD models of aneurysm flow during exercise. Zero-pressure boundary conditions were imposed at all outlets.

3. RESULTS

3.1. **Cohort statistics for flow variables.** Summary statistics of the Lido cohort are presented in Table 1. Differences between the sexes were observed in body size, left ventricular volume/mass, and carotid artery diameters. Carotid flow velocity waveforms were extracted from both ICA-L and ICA-R for $N = 92$ study participants. For $N = 11$ participants carotid examination failed in either one or both sides and no signal could be analysed. The log-transformed carotid flow rates after subtracting the time-averaged mean flow are presented in Fig. 3, for men and women separately. The coefficient of variation in the time-averaged flow was 34% for ICA-L and 39% for ICA-R, indicating large between-subjects variability. Qualitative evaluation of the cohort mean waveforms indicated that a more prominent dicrotic notch was present in males than in females. It is clear that using a single "normative" waveform to characterise this cohort will not produce credible CFD simulations.

3.2. **Between-subjects flow variability -model.** The mean flow rate of each carotid waveform was computed and the values used to fit the log-linear mixed effects model for $\overline{y}_{bs}$. The model fit is represented graphically in Fig. 4. The estimated effects for men and women in the ICA-L and ICA-R are given in Table 2. The fixed effect for height was statistically significant in women ($\beta_{h,L} = 4.165$, $p < 0.001$ and $\beta_{h,R} = 2.944$, $p = 0.01$), but not in men ($\beta_{h,L} = -0.224$, $p = 0.0825$ and $\beta_{h,R} = 0.200$, $p = 0.886$). In previous studies, cardiac stroke volume was associated with height following an allometric scaling law with power $\beta_h = 2.04$ (in adults) [4].

After subtracting the time-averaged component from the log-transformed ultrasound signals, $\ell = 18$ landmark points were selected on the waveform. Manual adjustment was required to ensure the positive definiteness of the covariance matrix (4). Once the Gaussian process models were trained for both men and women, they were used to generate a virtual waveform sample of 103 cases. The statistics of this virtual cohort were compared to the original cohort by applying the Kolmogorov-Smirnov -test (Table 3). The distribution of flow parameters in the resulting virtual cohort was statistically indistinguishable from the original cohort, indicating successful model training.

TABLE 1. Demographics and carotid measurements in an elderly cohort. Differences between the sexes are exhibited in body size and mass, left ventricle size and mass, and carotid artery diameters. Univariate p-values were computed by one-way ANOVA. Statistical significance with $p < 0.05$ denoted by * and with $p < 0.001$ denoted by **.

Demographics	Male	Female	p-value
N	41	62	
Age [y]	73 (9)	74 (6)	0.691
Height [cm]	174 (7)	161 (7)	$< 0.001^{**}$
Weight [kg]	80 (13)	65 (12)	$< 0.001^{**}$
Body-mass index	26.5 (3.3)	25.0 (3.8)	0.041^{*}
Carotid arteries			
Intima-media thickness CCA-L [mm]	0.87 (0.20)	0.83 (0.18)	0.302
Intima-media thickness CCA-R [mm]	0.88 (0.21)	0.84 (0.17)	0.329
Mean time-averaged velocity ICA-L [cm/s]	17.5 (3.9)	19.6 (5.3)	0.031^{*}
Mean time-averaged velocity ICA-R [cm/s]	18.2 (4.8)	18.9 (5.1)	0.491
Mean time-averaged velocity CCA-L [cm/s]	21.5 (6.4)	20.8 (4.9)	0.558
Mean time-averaged velocity CCA-R [cm/s]	21.5 (6.1)	19.6 (5.2)	0.101
Mean time-averaged velocity ECA-L [cm/s]	16.3 (5.2)	14.9 (4.2)	0.144
Mean time-averaged velocity ECA-R [cm/s]	16.6 (5.7)	16.3 (5.4)	0.763
Diameter ICA-L [mm]	7.1 (1.0)	6.6 (0.9)	0.009^{*}
Diameter ICA-R [mm]	7.0 (1.0)	6.5 (0.9)	0.009^{*}
Diameter CCA-L [mm]	7.0 (0.7)	6.6 (0.6)	0.001^{*}
Diameter CCA-R [mm]	7.1 (0.8)	6.7 (0.6)	0.002^{*}
Diameter ECA-L [mm]	5.0 (0.5)	4.6 (0.6)	0.002^{*}
Diameter ECA-R [mm]	4.9 (0.5)	4.6 (0.6)	0.010^{*}
Mean time-averaged flow rate ICA-L [ml/min]	429 (135)	411 (149)	0.526
Mean time-averaged flow rate ICA-R [ml/min]	437 (169)	382 (148)	0.087

3.3. **Study on the effect of exercise on aneurysm flow.** Flow variability in the host artery (either the internal carotid, middle cerebral, or posterior communicating artery) during rest and exercise was measured with two different indicators: mean flow (FLOW) and pulsatility index (PI). The variabilities of these indicators as well as the WSS-related quantities measured in the aneurysm are reported in in Table 4. Due to the effects of the CARS, FLOW only fluctuated moderately ($< 10\%$) even when the HR was increased considerably. Meanwhile, the PI increased by over 100% in certain cases. In practice, all WSS-related indicators (TAWSS, OSI, rTransWSS) experienced on average an increase when moving from rest to exercise (Table 4). By far the largest increase was observed in OSI, which more than doubled on average during exercise. rTransWSS was considerablly less sensitive to flow fluctuations, being only somewhat more sensitive than TAWSS. In our previous study [19] TransWSS was similarly found to be a smoother measure of WSS fluctuations.

Changes in the absolute values of WSS and OSI might have relatively little physiological meaning unless critical thresholds are met for upregulating atheroprotective (for

TABLE 2. Parameters of the mixed effects model for $\overline{y}_{bs}$, their 95%-confidence intervals, and p-values. Height had a statistically significant effect in women but not in men. Statistical significance with $p < 0.05$ denoted by * and with $p < 0.001$ denoted by **.

Model parameter, men	Value	Confidence interval	p-value
Time-averaged flow rate ICA-L, β_0	6.077	$(4.952 - 7.201)$	$< 0.001^{**}$
Time-averaged flow rate ICA-L, β_h	-0.224	$(-2.242 - 1.793)$	0.825
Time-averaged flow rate ICA-R, β_0	5.875	$(4.330 - 7.421)$	$< 0.001^{**}$
Time-averaged flow rate ICA-R, β_h	0.200	$(-2.573 - 2.973)$	0.886
Stdev of residuals ICA-L, σ_L	0.275		
Stdev of residuals ICA-R, σ_R	0.378		

Model parameter, women	Value	Confidence interval	p-value
Time-averaged flow rate ICA-L, β_0	3.986	$(2.982 - 4.990)$	$< 0.001^{**}$
Time-averaged flow rate ICA-L, β_h	4.165	$(2.052 - 6.277)$	$< 0.001^{**}$
Time-averaged flow rate ICA-R, β_0	4.506	$(3.452 - 5.559)$	$< 0.001^{**}$
Time-averaged flow rate ICA-R, β_h	2.944	$(0.727 - 5.160)$	0.010^{*}
Stdev of residuals ICA-L, σ_L	0.305		
Stdev of residuals ICA-R, σ_R	0.320		

TABLE 3. Flow parameters measured by ultrasound versus simulated by the between-subjects variability model (1), p-values computed by the Kolmogorov-Smirnov -test. Statistical significance with $p < 0.05$ denoted by * and with $p < 0.001$ denoted by **.

Flow parameter, women	Ultrasound	Model (1)	p-value
Time-averaged flow rate ICA-L [ml/min]	$433\ (146)$	$438\ (159)$	0.953
Time-averaged flow rate ICA-R [ml/min]	$409\ (135)$	$414\ (149)$	0.964
Pulsatility index ICA-L	$1.14\ (0.24)$	$1.16\ (0.24)$	0.475
Pulsatility index ICA-R	$1.20\ (0.27)$	$1.22\ (0.24)$	0.146
Resistivity index ICA-L	$0.65\ (0.07)$	$0.65\ (0.07)$	0.483
Resistivity index ICA-R	$0.66\ (0.07)$	$0.67\ (0.07)$	0.277

Flow parameter, men	Ultrasound	Model (1)	p-value
Time-averaged flow rate ICA-L [ml/min]	$424\ (118)$	$425\ (119)$	0.992
Time-averaged flow rate ICA-R [ml/min]	$454\ (177)$	$455\ (175)$	0.906
Pulsatility index ICA-L	$1.29\ (0.30)$	$1.31\ (0.27)$	0.315
Pulsatility index ICA-R	$1.29\ (0.27)$	$1.30\ (0.25)$	0.884
A Resistivity index ICA-L	$0.68\ (0.07)$	$0.68\ (0.06)$	0.850
Resistivity index ICA-R	$0.68\ (0.07)$	$0.69\ (0.06)$	0.938

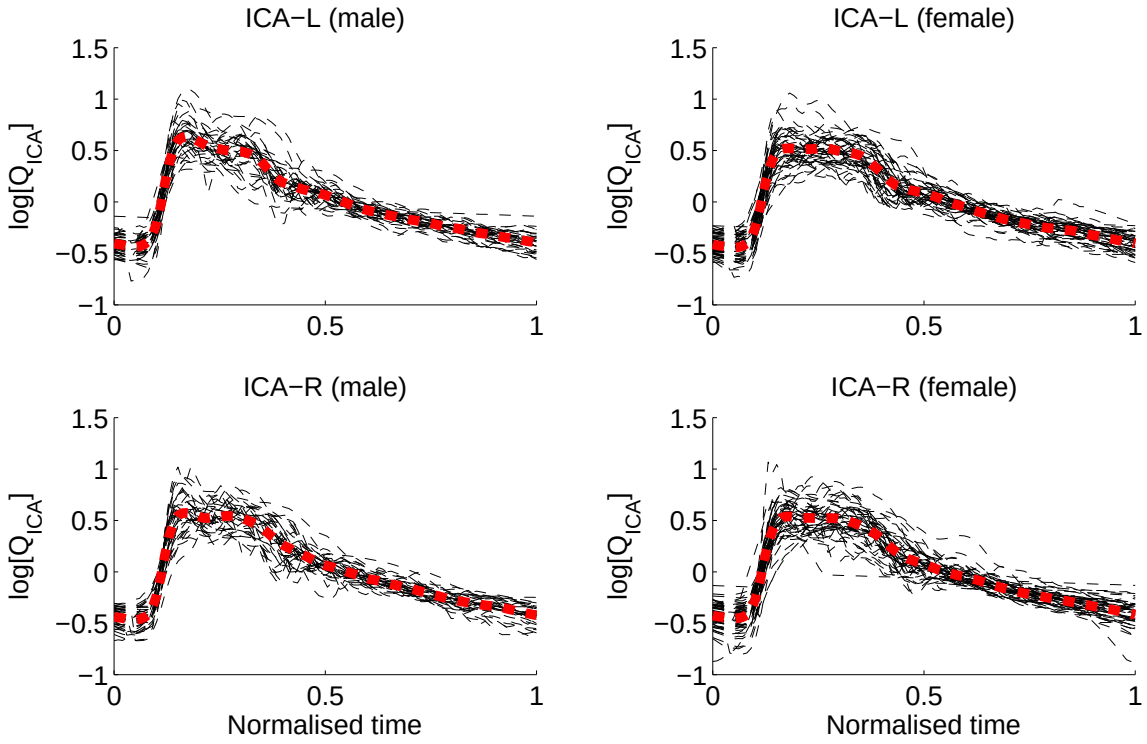

FIGURE 3. Log-transformed ICA flow waveforms in the study cohort in males (left column, $N = 38$) and females (right column, $N = 52$) after subtracting the temporal mean from each signal. Cohort mean waveform overlaid in red.

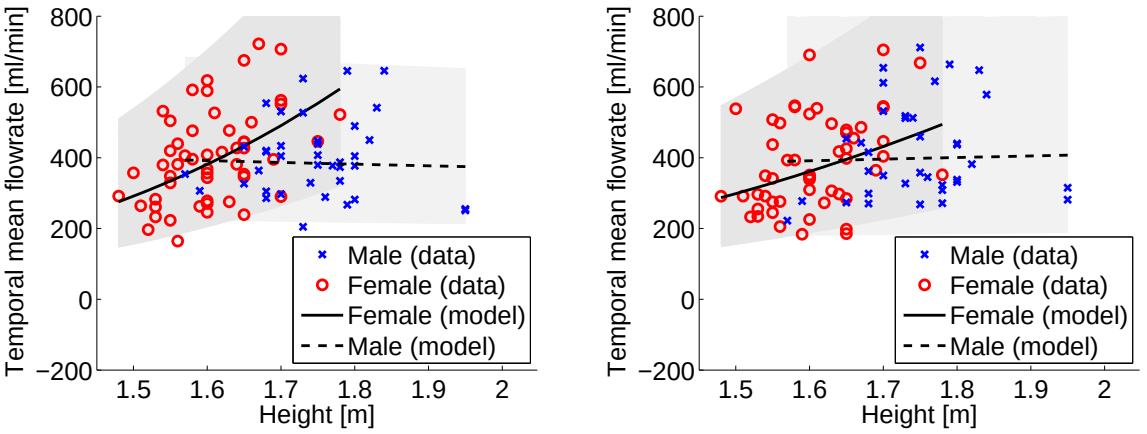

FIGURE 4. Mixed-effects log-linear model for temporal mean flow in the ICA-L (left) and ICA-R (right). Separate models are trained for males and females. Shaded area represents the 95% confidence intervals.

high TAWSS) or inflammatory pathways (low TAWSS and high OSI) in the endothelium. Therefore, we also studied areas of low TAWSS (defined as TAWSS < 0.4 Pa) and high OSI (defined as OSI > 0.4) relative to the total area of the aneurysmal sac.

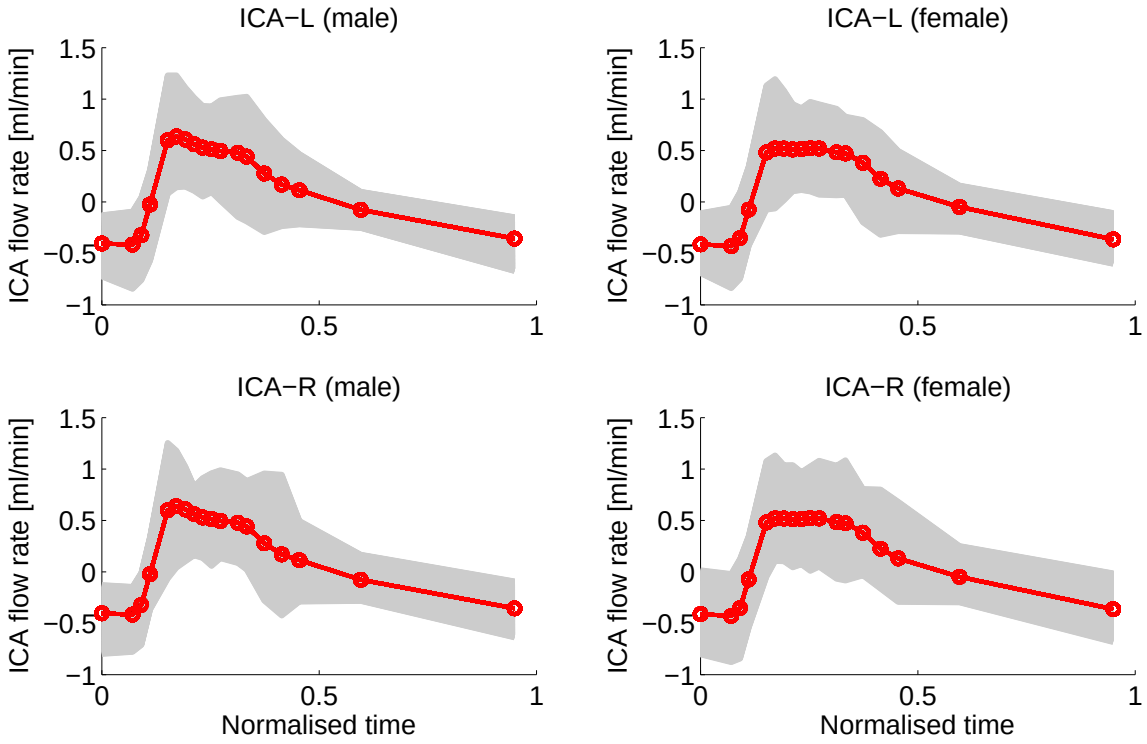

FIGURE 5. Gaussian process model for ICA flow fluctuation term in males (left column, $N = 38$) and females (right column, $N = 52$). Process mean waveform and landmarks overlaid in bold, variability bounds in gray.

Their changes are also reported in Table 4. It was observed that relative area of low TAWSS decreased on average, while the relative area of high OSI increased. To understand better the interplay of TAWSS and OSI, in Fig. 6 we present the case of a 41-year-old woman with a posterior communicating artery aneurysm. In this case, a large increase in host vessel pulsatility (ΔPI $= 102\%$) lead to a corresponding large increase in TAWSS (ΔTAWSS $= 39\%$) and OSI (ΔOSI $= 129\%$). It should be noted that OSI tends to be a spatially concentrated measure of flow variability, so that even a large increase in OSI only effects a small part of the aneurysmal wall. At the same time, while TAWSS increased in most regions it remained low in the region where OSI was simultaneously elevated. Thus the actual change in rupture risk should be evaluated based on a combined informations about TAWSS and WSS pulsatility indicators, including analysis of the spatial patterns of WSS.

Linear correlations between changes in flow vs. changes in WSS are reported in Table 5. It was found that, on average, TAWSS increases were associated incresses in both FLOW and PI, while the correlations between flow and OSI/rTransWSS changes were not statistically significant.

4. DISCUSSION

Computational fluid dynamics modelling is a promising tool for virtual treatment planning in cardio- and cerebrovascular disease, but requires patient-specific boundary

TABLE 4. Within-subject variability of flow- and WSS-related quantities in $N = 54$ intracranial aneurysms. Values given are cohort means (std. dev. in parentheses).

Indicator	Rest	Exercise	Relative difference
FLOW [ml/min]	240 (99)	245 (109)	2.00% (2.22%)
PI	1.18 (0.00)	2.13 (0.16)	80.3% (13.5%)
TAWSS	4.78 (4.17)	5.78 (4.93)	27.2% (19.6%)
OSI	0.027 (0.023)	0.053 (0.035)	124.0% (84.1%)
rTransWSS	0.168 (0.069)	0.240 (0.084)	48.1% (29.3%)
rArea Low TAWSS [%]	12.87 (22.07)	7.42 (15.04)	-58.6% (27.8%)
rArea High OSI [%]	2.30 (2.60)	5.09 (5.37)	165% (143%)

TABLE 5. Correlation coefficients between flow variability in the host artery (ICA) and WSS variability in $N = 54$ intracranial aneurysm.

Comparison	Pearson's ρ	p-value
ΔFLOW vs. ΔTAWSS	0.277	0.043*
ΔFLOW vs. ΔOSI	−0.132	0.340
ΔFLOW vs. ΔrTransWSS	−0.100	0.473
ΔFLOW vs. ΔrAreaLowTAWSS	−0.276	0.069
ΔFLOW vs. ΔrAreaHighOSI	−0.064	0.649
ΔPI vs. ΔTAWSS	0.430	0.001*
ΔPI vs. ΔOSI	−0.200	0.148
ΔPI vs. ΔrTransWSS	−0.225	0.102
ΔPI vs. ΔrAreaLowTAWSS	−0.183	0.237
ΔPI vs. ΔrAreaHighOSI	−0.101	0.469

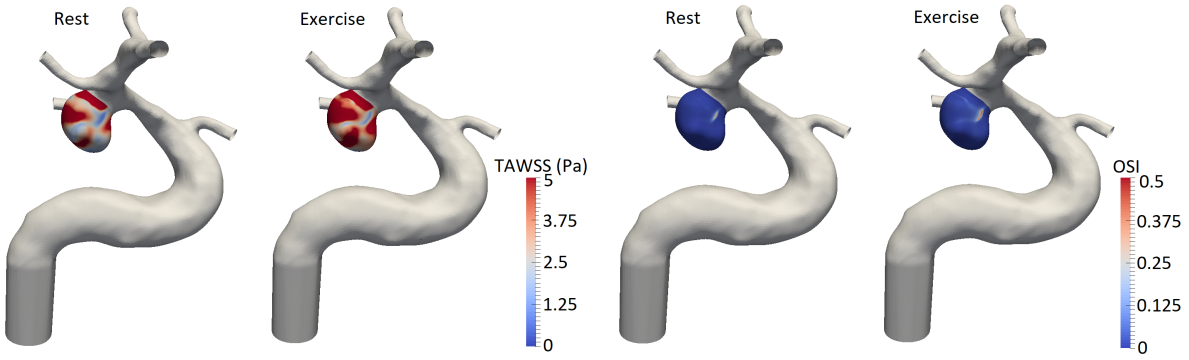

FIGURE 6. Example of flow in a posterior communicating artery aneurysm of a 41-year old female where a large increase in host vessel pulsatility (ΔPI $= 102\%$) leads to corresponding large increases in TAWSS (ΔTAWSS $= 39\%$) and OSI (ΔOSI $= 129\%$).

conditions to achieve results that are relevant to the specific patient's physiology. If normative flow boundary conditions are used instead, derived quantities of flow, such as WSS, may incur large errors and uncertainties. In the context of intracranial aneurysm

flow modelling, previous meta-analysis [18] showed that the use of patient-unspecific boundary conditions leads to a moderate-sized effect (Hedges' $g = 0.30$) when evaluating WSS patterns on the aneurysmal endothelium. This uncertainty can be multiplied by the presence of within-subject flow variability. However, in clinical practice only a single flow measurement is usually performed and no estimate of systemic variability is available to guide the modeller as to the variability in the flow measurements.

We developed a within-subject flow variability model that mimics the response of the cerebral autoregulation system to cardiac output variability. This model can be used to extend a single baseline carotid flow measurement to a range of CBF experienced during the person's daily activities. As a concrete example, we performed CFD simulations in 54 intracranial aneurysms where the intra-subject flow variability model was used to generate waveforms at rest and during physical activity. Our results showed that physiological changes in CBF during increased physical activity may induce fluctuations an order of magnitude higher in certain WSS-related quantities, such as OSI (a 2% mean increase in flow lead to a 124% mean increase in OSI in our virtual cohort). This indicates that OSI may be too sensitive to flow uncertainty to be reliably used for rupture-risk evaluation. A partial recipe to this problem is to use alternative WSS indicators that are robust to flow fluctuations. Specifically, we showed that TransWSS was less sensitive to flow fluctuations than OSI, so that if both indicators are equally informative for the rupture risk then TransWSS should be preferred over OSI.

Sometimes it is simply not feasible to perform patient-specific flow measures in all the relevant locations of the vascular tree. In such cases, using normative flow values may be a necessity, but the uncertainty created by missing patient-specific measurements should be properly quantified. Recent studies [5, 19, 25] have looked at between-subjects cerebral flow variability by combining data and mathematical modelling to quantify the CBF uncertainty. We developed a data-driven between-subjects flow variability modelfor ICA flow in elderly dementia patients and age-matched controls. The model was an extension of our previously developed model [19] but also included a fixed-effects model using height and sex as predictors for time-averaged mean flow. By training separate models for men and women, sex-specific differences of the cerebrovascular physiology can be studied.

Besides patient-specific models, a separate paradigm that has arisen lately is what we call "*population-specific modelling*". Instead of modelling the flow in a single patient, we generate a virtual population of waveforms that matches the statistical distribution of flow observed in a real patient cohort. The utility of virtual populations lies in the idea of *virtual in silico trials*, where medical treatments and devices can be tested using computer simulation. This can help reduce the size of actual clinical trials. By combining vascular surface models from a real cohort of patients and a between-subjects flow variability model, we can generate *virtual chimera patients* that extend the cohort beyond that which would be available with purely patient-specific data collection. It has been acknowledged that virtual patient models must incorporate both patient variability and the model uncertainty to augment clinical trials [7]. Our model provides one of the necessary ingredients to successful virtual trials of cerebrovascular interventions.

Limitations: Our data-driven model for between-subjects CBF variability was based on ~ 100 participants from an ethnically homogeneous cohort (retirees from an island community in the Mediterranean). As data from larger, cross-sectional population studies become available (e.g. the UK Biobank project [16]), the models can be retrained for

increased coverage and to achieve actual population-specific, not just cohort-specific models. The within-subject CBF variability was controlled by a simple autoregulation model that only considers short-term effects. Long-term response to chronic disruptions in CBF, such as cardiac disease, should be modelled using a more advanced autoregulation model.

ACKNOWLEDGEMENTS

We acknowledge A. Venneri, M. Mitolo, and F. Meneghello from IRCCS San Camillo as well as the @neurIST project for the clinical data collection, and M. Lange for assistance in the data processing. T. Lassila, A. Sarrami-Foroushani, and A.F. Frangi were funded by the H2020 Programme project InSilc *"In-silico trials for drug-eluting BVS design, development and evaluation"* (H2020-SC1-2017-CNECT-2-777119). T. Lassila and A.F. Frangi were funded by the 7th Framework Programme project VPH-DARE@IT *"Virtual Physiological Human: DementiA Research Enabled by IT"* (FP7-ICT-2011-5.2-601055). All authors declare no conflicts of interest exist.

REFERENCES

[1] Anderson, A.E., B.J. Ellis, and J.A. Weiss. Verification, validation and sensitivity studies in computational biomechanics. *Comput. Methods Biomech. Biomed. Eng.*, 10(3):171–184, 2007.

[2] Biehler, J., S. Kehl, M.W. Gee, F. Schmies, J. Pelisek, A. Maier, C. Reeps, H.-H. Eckstein, and W.A. Wall. Probabilistic noninvasive prediction of wall properties of abdominal aortic aneurysms using Bayesian regression. *Biomech. Model. Mechanobiol.*, 16(1):1–17, 2016.

[3] Boccadifuoco, A., A. Mariotti, S. Celi, N. Martini, and M.V. Salvetti. Impact of uncertainties in outflow boundary conditions on the predictions of hemodynamic simulations of ascending thoracic aortic aneurysms. *Comput. Fluids*, 165:96–115, 2018.

[4] de Simone, G., R.B. Devereux, S.R. Daniels, G. Mureddu, M.J. Roman, T.R. Kimball, R. Greco, S. Witt, and F. Contaldo. Stroke volume and cardiac output in normotensive children and adults. *Circulation*, 95(7):1837–1843, 1997.

[5] Durka, M.J., I.H. Wong, D.F. Kallmes, D. Pasalic, F. Mut, M. Jagani, P.J. Blanco, J.R. Cebral, and A.M. Robertson. A data-driven approach for addressing the lack of flow waveform data in studies of cerebral arterial flow in older adults. *Physiol. Measur.*, 39(1):015006, 2018.

[6] Ford, M.D., N. Alperin, S.H. Lee, D.W. Holdsworth, and D.A. Steinman. Characterization of volumetric flow rate waveforms in the normal internal carotid and vertebral arteries. *Physiol. Measur.*, 26(4):477, 2005.

[7] Haddad, T., A. Himes, L. Thompson, T. Irony, R. Nair, et al. Incorporation of stochastic engineering models as prior information in Bayesian medical device trials. *J. Biopharm. Stat.*, 27(6):1089–1103, 2017.

[8] Holdsworth, D.W., C.J.D. Norley, R. Frayne, D.A. Steinman, and B.K. Rutt. Characterization of common carotid artery blood-flow waveforms in normal human subjects. *Physiol. Measur.*, 20(3):219, 1999.

[9] Huberts, W., S.G.H. Heinen, N. Zonnebeld, D.A.F. van den Heuvel, J.-P.P.M. de Vries, J.H.M. Tordoir, D.R. Hose, T. Delhaas, and F.N. van de Vosse. What is needed to make cardiovascular models suitable for clinical decision support? A viewpoint paper. *J. Comput. Sci.*, 24:68–84, 2018.

[10] Krejza J., P. Szydlik, D.S. Liebeskind, J. Kochanowicz, O. Bronov, Z. Mariak, and E.R. Melhem. Age and sex variability and normal reference values for the VMCA/VICA index. *Am. J. Neuroradiol.*, 26(4):730–735, 2005.

[11] Lassila, T., L.Y. Di Marco, M. Mitolo, V. Iaia, G. Levedianos, A. Venneri, and A.F. Frangi. Screening for cognitive impairment by model assisted cerebral blood flow estimation. *IEEE Trans. Biomed. Eng.*, 65(7):1654–1661, 2018.

[12] MacDonald, M.E., and R. Frayne. Phase contrast MR imaging measurements of blood flow in healthy human cerebral vessel segments. *Physiol. Measur.*, 36(7):1517, 2015.

[13] Mader, G., M. Olufsen, and A. Mahdi. Modeling cerebral blood flow velocity during orthostatic stress. *Ann. Biomed. Eng.*, 43(8):1748–1758, 2015.

[14] Marshall, I., P. Papathanasopoulou, and K. Wartolowska. Carotid flow rates and flow division at the bifurcation in healthy volunteers. *Physiol. Measur.*, 25(3):691, 2004.

[15] Meng, H., V.M. Tutino, J. Xiang, and A. Siddiqui. High WSS or low WSS? complex interactions of hemodynamics with intracranial aneurysm initiation, growth, and rupture: toward a unifying hypothesis. *Am. J. Neuroradiol.*, 35(7):1254–1262, 2014.

[16] Miller, K.L., F. Alfaro-Almagro, N.K. Bangerter, D.L. Thomas, E. Yacoub, J. Xu, A.J. Bartsch, S. Jbabdi, S.N. Sotiropoulos, J.L.R. Andersson, et al. Multimodal population brain imaging in the uk biobank prospective epidemiological study. *Nat. Neurosci.*, 19(11):1523, 2016.

[17] Ogoh, S., P.J. Fadel, R. Zhang, C. Selmer, Ø. Jans, N.H. Secher, and P. B. Raven. Middle cerebral artery flow velocity and pulse pressure during dynamic exercise in humans. *Am. J. Physiol. Heart. Circ. Physiol.*, 288(4):H1526–H1531, 2005.

[18] Sarrami-Foroushani, A., T. Lassila, and A.F. Frangi. Virtual endovascular treatment of intracranial aneurysms: models and uncertainty. *Wiley Interdiscip. Rev. Syst. Biol. Med.*, 9(4), 2017.

[19] Sarrami-Foroushani, A., T. Lassila, A. Gooya, A.J. Geers, and A.F. Frangi. Uncertainty quantification of wall shear stress in intracranial aneurysms using a data-driven statistical model of systemic blood flow variability. *J. Biomech.*, 49(16):3815–3823, 2016.

[20] Su, Y., A.M. Arbelaez, T.L.S. Benzinger, A.Z. Snyder, A.G. Vlassenko, M.A. Mintun, and M.E. Raichle. Noninvasive estimation of the arterial input function in positron emission tomography imaging of cerebral blood flow. *J. Cereb. Blood Flow Metab.*, 33(1):115–121, 2013.

[21] Valen-Sendstad, K., and D.A. Steinman. Mind the gap: impact of computational fluid dynamics solution strategy on prediction of intracranial aneurysm hemodynamics and rupture status indicators. *Am J Neuroradiol.*, 35(3):536–543, 2014.

[22] Villa-Uriol, M.C., G. Berti, D.R. Hose, A. Marzo, A. Chiarini, J. Penrose, J.M. Pozo, J.G. Schmidt, P. Singh, R. Lycett, et al. @neurIST: complex information processing toolchain for the integrated management of cerebral aneurysms. *Interface Focus*, page rsfs20100033, 2011.

[23] Vlak, M.H.M., G.J.E. Rinkel, P. Greebe, and A. Algra. Risk of rupture of an intracranial aneurysm based on patient characteristics: a case–control study. *Stroke*, 44(5):1256–1259, 2013.

[24] Vlak, M.H.M., G.J.E. Rinkel, P. Greebe, J.G. van der Bom, and A. Algra. Trigger factors and their attributable risk for rupture of intracranial aneurysms: a case-crossover study. *Stroke*, 42(7):1878–1882, 2011.

[25] Xiang, J., A.H. Siddiqui, and H. Meng. The effect of inlet waveforms on computational hemodynamics of patient-specific intracranial aneurysms. *J. Biomech.*, 47(16):3882–3890, 2014.